ChemPubSoc Europe

DOI: 10.1002/cphc.201200914

Strong Light-Molecule Coupling on Plasmonic Arrays of Different Symmetry

Adi Salomon, Shaojun Wang, James A. Hutchison, Cyriaque Genet, and Thomas W. Ebbesen*[a]

The strong coupling of porphyrin J-aggregates to plasmonic nanostructures of different symmetry is investigated. The nanostructures of higher symmetry show the strongest interaction with the molecular layer, suggesting that surface plasmon mode degeneracy plays an important role in the coupling efficiency. At high coupling strengths a new, weakly dispersive mode appears which has recently been predicted theoretically to be due to long-range energy transfer between molecules mediated by surface plasmons. These findings point to new ways for optimizing strong coupling and thereby realize its full potential for molecular and material science.

1. Introduction

Hybrid light–matter states can be formed by coherent interaction between an optical cavity mode and any form of matter with a resonant excited state transition.[1–4] The interaction may be envisaged as the rapid exchange of energy between an excited state of a material and the photonic structure which, in the limit of low loss, results in the splitting of the original transition into two new hybrid states, the upper (UP) and lower (LP) cavity-polaritons. The strength of the interaction can be estimated by the characteristic energy difference between UP and LP, the Rabi splitting ($\hbar\Omega_R$), which for a two-level oscillator and neglecting dissipation is given by Equation (1):

$$\hbar\Omega_R = 2(\mathbf{E}\cdot\mathbf{d}) \times \sqrt{n_{ph}+1} \quad (1)$$

where **d** is the transition dipole moment of the two-level oscillator, and **E** the amplitude of the cavity optical field. The splitting can still be observed in the absence of real photons ($n_{ph}=0$), due to interaction of the material with zero-point field fluctuations in the cavity. In this vacuum field regime, the Rabi splitting also scales with the number of oscillators (atoms or molecules, n_{osc}) interacting with the cavity as $\sqrt{n_{osc}}$.

The strong modification of the energy levels of a material due to light/matter hybridization has already been shown to affect relaxation pathways in the coupled system,[5,6] and more recently the rates of photochemical reactions.[7,8] The coherence length of the cavity-polariton states can extend to the micrometer range, of interest for long-distance energy transfer,[9–12] and their bosonic character makes them suitable for applications in polariton condensation and thresholdless lasing.[13] These hybrid states thus have the potential to greatly improve efficiencies in optoelectronic devices.[14,15]

Most studies of strong light–matter coupling continue to focus on optical microcavity structures, typically inorganic semiconductors or organic molecules sandwiched between planar mirrors.[4,7,8,16] Strong coupling using the optical modes of a plasmonic nanostructure arrays was demonstrated several years ago,[12,17,18] and strong coupling of organic excitons with plasmonic resonances have been achieved using other geometries (e.g. smooth metallic films in the Kretchsmann configuration,[19,20] metallic nanoparticles).[21] Further efforts towards a deeper understanding of strong coupling on plasmonic structures is justified as they provide surface-localized electromagnetic fields and are open to the environment, and thus can have advantages over the microcavity geometry for applications. Here we undertake such a study, focusing on the particular role of plasmonic array symmetry.

Experimental Section

Sub-wavelength hole arrays were milled by focused ion beam (FEI Dual Strata 235) in sputtered silver films of 260 nm thickness on glass substrates. The hole diameter was kept constant at 150 nm as the array period was varied. Layers of J-aggregates of 4,4′,4″,4‴-(porphine-5,10,15,20-tetrayl)tetrakis(benzenesulfonic acid) tetrasodium salt hydrate (Aldrich) and of the polycation poly(diallyldimethylammonium chloride) solution (average M_w 200 000–350 000, 20 wt.% in water, Aldrich) were alternately adsorbed onto 1 mm thick PDMS slabs using layer-by-layer assembly. Polyelectrolyte layers were deposited by soaking the PDMS slab for 10 min in a solution of PDDA (8×10^{-2} M) and NaCl (0.7 M) in deionized water. J-aggregate layers were deposited by soaking the PDMS slab for 10 min in a solution of H_2TPPS^{4-} (1×10^{-4} M) in H_2O, which had

[a] Dr. A. Salomon,[+] S. Wang, Dr. J. A. Hutchison, Dr. C. Genet, Prof. T. W. Ebbesen
ISIS
Université de Strasbourg and CNRS (UMR 7006)
Strasbourg (France)
E-mail: ebbesen@unistra.fr

[+] Current address
Chemical Physics Department
Weizmann Institute of Science
76100 Rehovot (Israel)

Supporting information for this article is available on the WWW under http://dx.doi.org/10.1002/cphc.201200914.

been previously sonicated for 5 min and then adjusted to have a pH of 1.5 using HCl, promoting J-aggregate formation. The polyelectrolyte was deposited first and between each subsequent layer deposition the substrate was rinsed with water (pH 1.5) and dried with nitrogen. To avoid two surfaces of PDMS being exposed to solution, one face of the PDMS slab was bonded to a glass substrate. The amount of J-aggregate deposited in each bilayer depends on the acidity of the J-aggregate solution between solution pH 1.0 and pH 2.0, affording another control for the final absorbance of the layer.

2. Results and Discussion

Figure 1 a shows the schematic of the hybrid organic/inorganic structure we chose for this study. A film of tetraphenylporphine tetrasulfonic acid (H_2TPPS^{4-}), which forms J-aggregates in acidic conditions (H_4TPPS^{2-}), is adsorbed to a nanostructured silver film (260 nm thick) which supports surface plasmon modes. The porphyrin J-aggregates typically have a rod-like shape with lengths in the micrometer range consisting of thousands of molecules.[22] In a previous study (e.g. ref. [6]), J-aggregated H_4TPPS^{2-} dispersed in PVA [poly(vinyl alcohol)] was deposited on nanostructured silver films by spin-casting. Here we chose instead to adhere the J-aggregate film, built up by layer-by-layer electrostatic deposition[15] on an elastomeric substrate, so as to confine the molecules in the region of highest field amplitude near the nanostructure surface, and to avoid any deleterious chemical effects on the Ag film from spin-casting solutions. Various numbers of bilayers of H_4TPPS^{2-}/poly(diallyldimethylammonium chloride) (PDDA) were absorbed on 1 mm thick poly(dimethylsiloxane) (PDMS) slabs (see the Experimental Section for details). The slab of PDMS with the molecular film was dried using a stream of nitrogen and then gently bonded to the Ag surface (Figure 1 a).

Absorption spectra of the J-aggregate films on PDMS as a function of H_4TPPS^{2-}/PDDA bilayer number are shown in Figure 1 b. Each bilayer is typically 3–5 nm thick.[23,24] The films exhibit two well-defined absorption bands in the visible region at 706 nm (1.76 eV) and at 491 nm (2.53 eV), with full width at half maximum (FWHM) of 56 nm and 29 nm respectively. The measured absorbance at the J-aggregate bands per bilayer adsorbed to the PDMS slab was sensitive to experimental conditions and varied from one run to another. However for any single series of adsorptions, the J-aggregate absorption increased linearly with the numbers of bilayers (inset, Figure 1 b). These high optical density films with well-defined absorptions are perfect for studying strong interactions with plasmonic substrates.

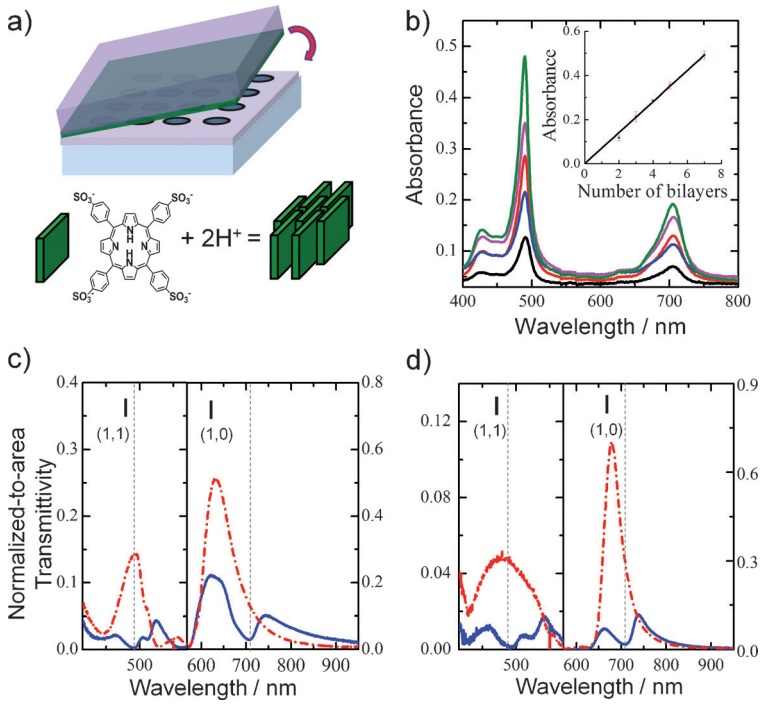

Figure 1. a) Schematic sub-wavelength hole array milled in a silver film on a glass substrate upon which is adsorbed J-aggregated H_4TPPS^{2-}/PDDA bilayers grown on a slab of PDMS. The structure of H_2TPPS^{4-} and the promotion of its J-aggregation by acidity are indicated. b) Absorption spectra of two, three, four, five, and seven J-aggregated H_4TPPS^{2-}/PDDA bilayers deposited on PDMS. The peak positions of the J-aggregate absorptions are at 706 nm (1.76 eV) and 491 nm (2.53 eV) respectively. Inset: Absorbance at 491 nm versus number of J-aggregate/PDDA bilayers on PDMS. c) Normal incidence transmission of a square hole array (Period 330 nm) when bonded to a 1 mm thick PDMS slab (red curve) and when bonded to a PDMS slab with J-aggregated H_4TPPS^{2-}/PDDA bilayers with absorbance 0.898 at 491 nm (blue curve). d) Normal incidence transmission of a hexagonal hole array (Period 430 nm) when bonded to a 1 mm thick PDMS slab (red curve) and when bonded to a PDMS slab with J-aggregated H_4TPPS^{2-}/PDDA bilayers with absorbance 0.898 at 491 nm adsorbed (blue curve). In Figure c) and d) the vertical scale is expanded to show clearly the interaction of the SP mode (1,1) with the 491 nm J-aggregate transition, the dashed vertical lines indicate the J-aggregate transition energies, and the short, solid vertical marks indicate the wavelengths of the SP modes estimated from Equation (3).

Surface plasmon polaritons (SPs) modes on sub-wavelength metallic hole arrays are generated via Bragg scattering according to Equation (2):[25,26]

$$\left|\vec{k}_{SP}\right| = \left|\vec{k}_{||} + i\vec{G}_x + j\vec{G}_y\right| \quad (2)$$

where $k_{||}$ is the in-plane wave vector component of the incident light, k_{SP} is the SP wave vector, $\vec{G}_x$ and $\vec{G}_y$ are the reciprocal lattice vectors ($|\vec{G}_x| = |\vec{G}_y| = 2\pi/P$, and P is the lattice period), and i and j are integers. One of the fascinating phenomena of such coupling is the observation of extraordinary optical transmission through holes with lateral dimensions which are smaller than half the wavelength of incident light.[25] The peak positions are associated with surface plasmon array excitations, with wavelength λ_{SP}, which can be described to a first approximation by Equation (3):

$$\lambda_{SP} = \frac{P}{C}\sqrt{\frac{\varepsilon_d \varepsilon_m}{\varepsilon_d + \varepsilon_m}} \quad (3)$$

where ε_m and ε_d are the permittivity of the metal and the dielectric material in contact, and C is given by $\sqrt{i^2 + j^2}$ for a square array, and $\sqrt{\frac{4}{3}(i^2 + ij + j^2)}$ for a hexagonal array. Equation (2) shows that tuning plasmonic modes to a desired frequency can be

easily achieved by changing the array's periodicity or by changing the angle of incident light [$k_{||}$ in Eq. (2)] for a fixed period. Equation (3) shows that changing the symmetry of the nanostructure provides a further tool for the systematic study of the interaction of molecular excited states with SP modes of different grating orders, and varying levels of degeneracy, as will be discussed further below.

The red curves in Figures 1 c,d show the transmission spectra through square and hexagonal arrays respectively when a slab of PDMS is adsorbed to the array surface (no J-aggregates present). The two transmission peaks are due to SP modes propagating at the second and the third Brillouin zones (BZ), respectively. The effect of PDMS adsorption compared to a metal/air interface is a strong enhancement of the lowest energy mode (noted as 1,0 here) and broadening of the next-highest energy mode (noted as 1,1) due to the presence of SPs on the upper and lower surfaces of the hole array (the refractive index of bulk PDMS and the glass substrate are 1.46 and 1.47 respectively at 633 nm, also see the Supporting Information). The periods of the arrays were chosen such that the (1,1) SP modes of the array were resonant with the 491 nm absorption band of the J-aggregate. Owing to the smaller lattice angle of hexagonal hole array, its (1,0) mode is then coincidentally also resonant with the 706 nm absorption of the J-aggregate.

The blue curves in Figures 1 c,d show the transmission spectra through square and hexagonal arrays respectively when a slab of PDMS/J-aggregate film was bonded to the surface of the arrays (absorbance of J-aggregate film was 0.898 at 491 nm). The splitting of the (1,1) mode due to interaction with the J-aggregate band at 491 nm is magnified for clarity. Note that the molecules interact mainly with the modes on the PDMS side. For the square array, the Rabi splitting of the (1,1) SP mode, 0.30 eV, is larger than the FWHM of the corresponding (1,1) mode, 0.19 eV. However for the hexagonal array the Rabi splitting (0.42 eV) is actually slightly smaller than the FWHM of the bare mode (ca. 0.51 eV). Nevertheless as shown below, all the other data (dispersion curves in the Supporting Information, concentration dependence, etc.) demonstrates that the strong coupling regime is reached. In addition the dip in the transmission spectrum is not solely the negative of the molecular absorption. This suggests that the SP (1,1) mode broadened by the coupling to the SP mode on the opposite interface may not always be a good reference for whether a system has entered the strong coupled regime. It can be noted that the single side mode is much narrower with a FWHM of 0.29 eV (Figure S1).

In Figure 2, the period dispersion at normal incidence is shown for two different coupling strengths wherein the adsorbed J-aggregate film absorbance at 491 nm was 0.460 (Figures 2 a,e) or 0.898 (Figures 2 c,g). The large Rabi splitting observed for the interaction between the J-aggregate absorption at 491 nm and the (1,1) SP mode observed is due primarily to the higher molecular extinction coefficient of the J-aggregate at that wavelength, but may also benefit from higher confinement of the (1,1) SP mode as compared to the (1,0) SP mode. Concentrating the J-aggregate in a thin layer ($<$ 50 nm)[23,24] at

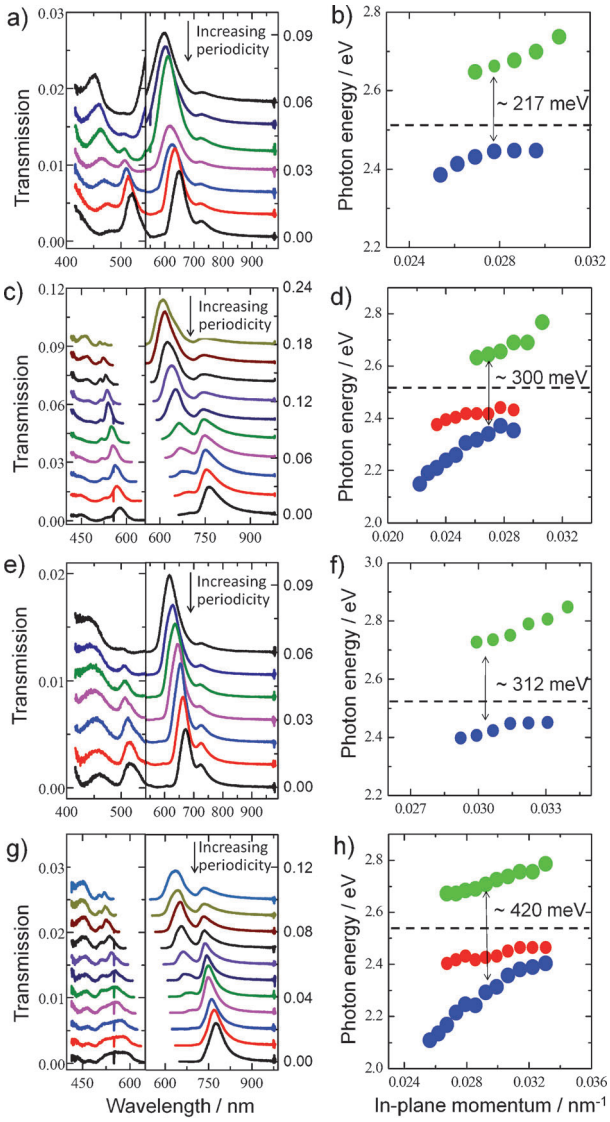

Figure 2. a) Normal incidence transmission spectra of a set of square hole arrays (Periods from 290 nm to 350 nm as indicated by the arrow) with PDMS/J-aggregate film adsorbed (absorbance 0.460 at 491 nm). b) Dispersion of the peaks observed in the region 400–550 nm in (a). The green and blue dots correspond to the upper (UP) and lower (LP) polariton bands respectively. The black dashed line is the J-aggregate 491 nm absorption energy. c) Normal incidence transmission spectra of a set of square hole arrays (Periods from 310 nm to 400 nm as indicated by the arrow) with PDMS/J-aggregate film adsorbed (absorbance 0.898 at 491 nm). d) Dispersion of the peaks observed in the region 400–550 nm in (c). The green and blue dots correspond to the UP and LP respectively, while the red dots correspond to the new, weakly-dispersive mode close to the molecular resonance. The black dashed line is the J-aggregate 491 nm absorption energy. e) Normal incidence transmission spectra of a set of hexagonal hole arrays (Periods from 370 nm to 420 nm as indicated by the arrow) with PDMS/J-aggregate film adsorbed (absorbance 0.460 at 491 nm). f) Dispersion of the peaks observed in the region 400–550 nm in (e). The green and blue dots correspond to the UP and LP respectively. The black dashed line is the J-aggregate 491 nm absorption energy. g) Normal incidence transmission spectra of a set of hexagonal hole arrays (Periods from 380 nm to 490 nm as indicated by the arrow) with PDMS/J-aggregate film adsorbed (absorbance 0.898 at 491 nm). h) Dispersion of the peaks observed in the region 400–550 nm in (g). The green and blue dots correspond to the UP and LP respectively, while the red dots correspond to the new, weakly-dispersive mode close to the molecular resonance. The black dashed line is the J-aggregate 491 nm absorption energy.

the array surface where the plasmon field has the greatest amplitude also maximizes interaction compared to spreading the aggregates over hundreds of nanometers in a host polymer matrix on the array. For instance, for the same porphyrin J-aggregate dispersed in 150 nm of poly(vinyl alcohol) on a silver hexagonal array with absorbance at 491 nm of 0.49, a Rabi splitting of 200 meV was measured.[6] The layer-by-layer J-aggregate film here with absorbance of 0.460 at 491 nm gives a splitting of 312 meV.

One of the important results of the optimization of strong coupling on these hole arrays is the observation of a new, weakly-dispersive transmission mode associated with the hybridization process and which appears both for the square and hexagonal arrays when the J-aggregate density is largest. This is shown in the dispersion curves in Figures 2 d,h. The peak lies between the upper and lower cavity polariton bands, slightly red-shifted from the maximum of the J-aggregate absorption (see red dots, Figure 2 d,h). The band remains weakly dispersive even at high momenta (high observation angles, see Figure S2), where the upper and lower cavity polariton bands disperse strongly. The peak vanishes at lower molecular densities independent of the absolute value of the Rabi splitting (compare Figures 2 b,d,f,h, and see also the spectra in Figures 3 a,b). This new feature of molecule–surface plasmon strong coupling on nanostructured arrays was predicted theoretically recently and attributed to a long-range energy transfer between J-aggregates, mediated by SPs.[27] We have also observed weakly dispersive transmission modes associated with molecular absorption bands when adsorbing a dense layer of J-aggregates within 30 nm of a nanostructured metal surface.[28] These systems are very different but the origin could be the same, a question which demands further exploration.

To understand the role of mode degeneracy on the Rabi splitting, we compared the J-aggregate absorption at 491 nm for the hexagonal and square arrays. Figure 3 c shows that for arrays of both symmetries, the degree of vacuum Rabi splitting has the well-known square root dependence on the absorbance of the material.[2,17] However, at any absorbance, the Rabi splitting is much greater for the hexagonal array. This points to a hitherto little-considered possibility—that the higher degeneracy of the plasmonic vacuum field can increase $\hbar\Omega_R$ in a similar way to the density of organic absorbers. Given the SP modes we have chosen in this study, the hexagonal array supports a 6-fold degeneracy, whilst the square array supports only a 4-fold degeneracy.[29]

In the absence of dissipation, the energies of the eigenstates $E_\pm$ (UP and LP) are, at resonance, given by Equation (4):

$$E_\pm = \frac{1}{2}(E_{SP} + E_{Ex}) \pm \frac{1}{2}\sqrt{4V^2} \quad (4)$$

so that [Eq. (5)]:

$$\hbar\Omega_R = \sqrt{4V^2} \quad (5)$$

where V is the interaction coupling strength between the SP mode energy E_{SP} and the molecular transition energy E_{Ex}. Each SP mode of the same frequency, that is, degenerate modes, will contribute to the coupling interaction. As a consequence, the Rabi splitting should depend on the SP mode degeneracy (n_d) as Equation (6):

$$\hbar\Omega_R = \sqrt{4n_dV^2} \quad (6)$$

We therefore might expect that the ratio of the Rabi splitting of the hexagonal and square arrays is $\sqrt{\frac{6}{4}} = 1.22$. The ratio derived experimentally, 1.41, is in good qualitative agreement considering this simplified model derived from symmetry considerations alone.

Surface plasmon field intensities may also play a role in the different Rabi splitting observed for the square and hexagonal arrays. Optimal field amplitudes occur on hole arrays when the hole diameter matches half the array period.[30] The hole diameter for all the experiments was kept constant at 150 nm, in order to suppress low-intensity transmission modes that result from SP coupling on each interface and which complicate band assignment (see the Supporting Information). Thus, the field amplitudes are more optimal for the square array (Period 330 nm) than for the hexagonal array (Period 440 nm) and cannot explain the greater Rabi splitting for hexagonal arrays. Independent of the particular conditions, we have noticed that for other dyes the Rabi splitting was always greater for the hexagonal array. The increase in degeneracy is akin to an increase in the density of optical states which should naturally increase the coupling strength.

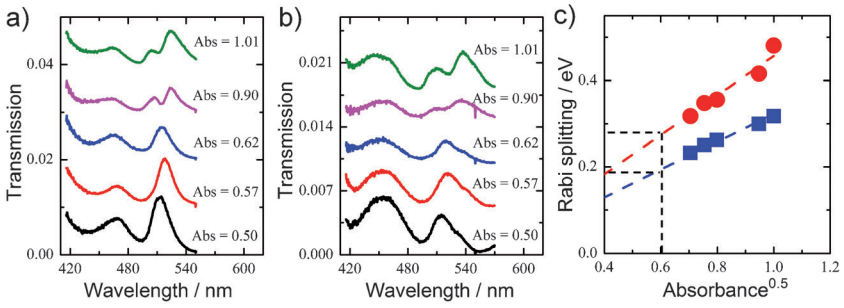

Figure 3. Normal incidence transmission spectra of a) square and b) hexagonal hole arrays upon increasing the adsorbed J-aggregate layer absorbance at 491 nm. At absorbance of 0.90 or higher, a new peak is observed between the two hybrid modes for both array symmetries. c) Rabi splitting values as a function of the square root of the J-aggregate absorbance at 491 nm for both hexagonal (circles) and square arrays (squares). The blue and red dashed lines are linear fits (slopes 0.323 and 0.457 for square and hexagonal arrays respectively). The black dashed lines indicate the minimum molecular film absorbance required to observe the Rabi splitting (strong coupling).

3. Conclusions

To conclude we used a combination of layer-by-layer and elastomeric deposition techniques to adsorb a J-aggregate in a thin layer directly at the surface of plasmonic arrays to maximize strong coupling. It was demonstrated that hybrid light–matter states with larger Rabi splitting could be achieved when using plasmonic nanostructures of higher symmetry, indicating that SP mode degeneracy is important for efficient coupling. A new weakly dispersive transmission mode was observed near the molecular resonance, which has been predicted theoretically to be associated with exciton–exciton hybridization. These findings point to new ways for optimizing strong coupling and thereby realize its full potential for molecular and materials science.

Acknowledgements

This research was funded by the ERC (grant no. 227577). S.W. acknowledges the support of the Chinese Scholarship Council (CSC).

Keywords: excitons · Rabi splitting · strong coupling · surface plasmons · symmetry

[1] S. Haroche, D. Kleppner, *Phys. Today* **1989**, *42*, 24.
[2] R. Houdré, *Phys. Status Solidi B* **2005**, *242*, 2167.
[3] W. L. Barnes, *J. Mod. Opt.* **1998**, *45*, 661.
[4] C. Weisbuch, M. Nishioka, A. Ishikawa, Y. Arakawa, *Phys. Rev. Lett.* **1992**, *69*, 3314.
[5] V. M. Agranovitch, M. Litinskaia, D. G. Lidzey, *Phys. Rev. B* **2003**, *67*, 085311.
[6] A. Salomon, C. Genet, T. W. Ebbesen, *Angew. Chem.* **2009**, *121*, 8904 – 8907; *Angew. Chem. Int. Ed.* **2009**, *48*, 8748 – 8751.
[7] T. Schwartz, J. A. Hutchison, C. Genet, T. W. Ebbesen, *Phys. Rev. Lett.* **2011**, *106*, 196405.
[8] J. A. Hutchison, T. Schwartz, C. Genet, E. Devaux, T. W. Ebbesen, *Angew. Chem.* **2012**, *124*, 1624; *Angew. Chem. Int. Ed.* **2012**, *51*, 1592.
[9] S. A. Guebrou, C. Symonds, E. Homeyer, J. C. Plenet, Yu. N. Gartstein, V. M. Agranovich, J. Bellessa, *Phys. Rev. Lett.* **2012**, *108*, 066401.
[10] D. G. Lidzey, D. D. C. Bradley, A. Armitage, S. Walker, M. S. Skolnick, *Science* **2000**, *288*, 1620.
[11] D. E. Gómez, K. C. Vernon, P. Mulvaney, T. J. Davis, *Appl. Phys. Lett.* **2010**, *96*, 073108.
[12] J. Bellessa, C. Bonnand, J. C. Plenet, J. Mugnier, *Phys. Rev. Lett.* **2004**, *93*, 036404.
[13] D. Snoke, P. Littlewood, *Phys. Today* **2010**, *63*, 42.
[14] O. Benson, *Nature* **2011**, *480*, 193.
[15] J. R. Tischler, M. S. Bradley, Q. Zhang, T. Atay, A. Nurmikko, V. Bulović, *Org. Electron.* **2007**, *8*, 94.
[16] D. G. Lidzey, D. D. C. Bradley, M. S. Skolnick, T. Virgili, S. Walker, D. M. Whittaker, *Nature* **1998**, *395*, 53.
[17] J. Dintinger, S. Klein, F. Bustos, W. L. Barnes, T. W. Ebbesen, *Phys. Rev. B* **2005**, *71*, 035424.
[18] P. Vasa, C. Ropers, R. Pomraenke, C. Lienau, *Laser Photonics Rev.* **2009**, *3*, 483.
[19] G. P. Wiederrecht, J. E. Hall, A. Bouhelier, *Phys. Rev. Lett.* **2007**, *98*, 083001.
[20] T. K. Hakala, J. J. Toppari, A. Kuzyk, M. Pettersson, H. Tikkanen, H. Kunttu, P. Törmä, *Phys. Rev. Lett.* **2009**, *103*, 053602.
[21] Y.-W. Hao, H.-Y. Wang, Y. Jiang, Q.-D. Chen, K. Ueno, W.-Q. Wang, H. Misawa, H.-B. Sun, *Angew. Chem.* **2011**, *123*, 7970; *Angew. Chem. Int. Ed.* **2011**, *50*, 7824.
[22] A. D. Schwab, D. E. Smith, C. S. Rich, E. R. Young, W. F. Smith, J. C. de Paula, *J. Phys. Chem. B* **2003**, *107*, 11339.
[23] P. G. Van Patten, A. P. Shreve, R. J. Donohoe, *J. Phys. Chem. B* **2000**, *104*, 5986.
[24] K. Ariga, Y. Lvov, T. Kunitake, *J. Am. Chem. Soc.* **1997**, *119*, 2224.
[25] T. W. Ebbesen, H. J. Lezec, H. F. Ghaemi, T. Thio, P. A. Wolff, *Nature* **1998**, *391*, 667.
[26] C. Genet, T. W. Ebbesen, *Nature* **2007**, *445*, 39.
[27] A. Salomon, R. J. Gordon, Y. Prior, T. Seideman, M. Sukharev, *Phys. Rev. Lett.* **2012**, *109*, 073002.
[28] J. A. Hutchison, D. M. O'Carroll, T. Schwartz, C. Genet, T. W. Ebbesen, *Angew. Chem.* **2011**, *123*, 2133; *Angew. Chem. Int. Ed.* **2011**, *50*, 2085.
[29] In our case, at normal incidence, we tune the periodicity of both square and hexagonal plasmonic arrays so that plasmon wavelength (λ_{SP}) matches the absorption of the molecules, where λ_{SP} is related to the period (P) as per Equation (3). We chose, for both square and hexagonal arrays, to work with the second resonant modes of the array (the 1,1 modes in Figure 1 c,d) which involve the gamma points of the 3rd Brillouin zone, given by $C = \sqrt{2}$ for a square array and $C = 2$ for a hexagonal array [see Eq. (3)]. For a square array the irreducible representations in the 3rd Brillouin zone of the gamma point (C_{4v} group symmetry) tells us that at this wavelength, two modes are non-degenerate and one mode is doubly degenerate. In our density picture this would be associated with a 4-fold degeneracy. The same analysis for a hexagonal array (C_{6v} group symmetry) tells us that the irreducible representations of the gamma point consist of 2 non-degenerate modes and two doubly degenerate modes, thus 6-fold degeneracy. We associate these full degeneracy numbers with the optical mode density on the surface which contributes to the Rabi splitting.
[30] E. Laux, C. Genet, T. W. Ebbesen, *Opt. Express* **2009**, *17*, 6920.

Received: November 6, 2012
Published online on April 10, 2013